



# CHESTER

Compressed Heat Energy  
Storage for Energy  
from Renewable sources

## Detailed design of the high temperature TES laboratory prototype

PROJECT	<b>CHESTER</b>
PROJECT NO.	<b>764042</b>
DELIVERABLE NO.	<b>D3.3</b>
DOCUMENT VERSION	<b>V2</b>
DOCUMENT PREPARATION DATE	<b>27-09-2019</b>
RESPONSIBLE PARTNER	<b>DLR</b>
DISSEMINATION LEVEL	<b>Public</b>

Type of Deliverable		
<b>R</b>	Document, Report	<b>X</b>
<b>DEM</b>	Demonstrator, pilot, prototype	
<b>DEC</b>	Websites, patent fillings, videos, etc.	
<b>OTHER</b>		
<b>ETHICS</b>	Ethics requirements	
<b>ORDP</b>	Open Research Data Pilot	



*This project has received funding from the European Union's Horizon 2020 research and innovation programme under grant agreement No. 764042.*

*This deliverable reflects only the author's views and neither Agency nor the Commission are responsible for any use that may be made of the information contained therein.*

EC Grant Agreement	No.764042
Project Acronym	CHESTER
Project Title	Compressed Heat Energy Storage for Energy from Renewable sources
Programme	HORIZON 2020
Start Date of Project	01-04-2018
Duration	48 Months

#### Financial/Administrative Coordinator

Project Coordinator Organization Name	TECNALIA
Address	Parque Tecnológico de Bizkaia C/Astondo, Edificio 700 (Spain)
Phone Numbers	+34 946 430 850
E-mail Address	<a href="mailto:nora.fernandez@tecnalia.com">nora.fernandez@tecnalia.com</a>
Project web-site	<a href="http://www.chester-project.eu">www.chester-project.eu</a>

#### Version Management

Filename	Deliverable No. 3.3: Detailed design of the high temperature TES laboratory prototype		
Author(s)	T. Weller, H. Jockenhöfer, M. Fiss, D. Bauer		
Reviewed by	S. Ochoa de Eribe		
Approved by	Felipe Trebilcock		
Revision No.	Date	Author	Modification description
RV 1	03-09-2019	F. Trebilcock	WP3 leader first review with comments
RV 2	11-09-2019	T. Weller	High Quality Deliverable version available
RV 3	24-09-2019	S. Ochoa	Reviewed with minor corrections
RV 4	27-09-2019	H. Jockenhöfer	Corrected according to the review
RV 5	27-09-2019	N. Fernandez	Final formatting

## Contents

1.	Introduction.....	7
1.1.	Executive Summary .....	7
1.2.	Purpose and Scope .....	7
1.3.	Methodology .....	7
1.4.	Structure of the document.....	7
1.5.	Relations with other deliverables.....	8
2.	Description of the Thermal Energy Storage System.....	9
2.1.	General description of the HT-TESS.....	9
2.2.	Definition of the main design parameters .....	10
2.3.	Basic design concept definition .....	10
2.3.1.	Latent heat thermal energy storage (LH-TES) .....	10
2.3.2.	Sensible heat thermal energy storage (SH-TES) .....	14
3.	HT-TESS Thermodynamic Analysis and Modelling .....	15
3.1.	LH-TES.....	15
3.1.1.	Development and extension of numerical models .....	15
3.1.2.	Parameter study of latent heat storage component.....	17
3.1.3.	Thermodynamic analysis of the finned tubes .....	25
3.2.	SH-TESS .....	27
3.2.1.	Thermodynamic analysis of the SH-TESS.....	27
3.3.	Discussion .....	28
3.3.1.	Parameter study of the LH-TES.....	28
3.3.2.	Thermodynamic analysis of the finned tubes .....	28
3.3.3.	Thermodynamic analysis of the SH-TESS.....	29
4.	HT-TESS Design and Manufacturing .....	30
4.1.	Detailed design of LH-TES.....	30
4.2.	Detailed design of SH-TESS.....	32
4.3.	Manufacturing of the HT-TESS .....	34
5.	Conclusions.....	35
	<b>References.....</b>	<b>36</b>

## List of Figures

Figure 1: Conceptual diagram of the HT-TESS.....	9
Figure 2: Summary of thermodynamic states at nominal point operation.....	10
Figure 3: Fundamental heat transfer mechanism in a LH-TES during discharging and typical operation characteristics.....	11
Figure 4: Radial (left) and axial (center and right) finned tubes for LH-TES application (source DLR).....	12
Figure 5: Impact of operation strategy (multiple pass and single pass) on LH-TES characteristic.....	12
Figure 6: Simplified schematic of a latent heat thermal energy storage based on a storage unit developed in another project (Contract number 03ESP011, ©FW Brökelmann).....	13
Figure 7: Side view and top view of a control volume in cylindrical coordinates [4].....	16
Figure 8: Spatial discretization of the two-phase flow model on the control volume nodes N, P and S.....	17
Figure 9: Temperature of the working fluid at the lower tube exit during charging for the nominal diameter DN 10 .....	20
Figure 10: Temperature of the working fluid at the lower tube exit during charging for the nominal diameter DN 20 .....	21
Figure 11: Heat transfer rate of the LH-TES unit during charging for the nominal tube diameter DN 10 .....	21
Figure 12: Heat transfer rate of the LH-TES unit during charging for the nominal tube diameter DN 20 .....	22
Figure 13: Steam temperature at the upper tube exit during discharging for the nominal diameter DN 10.	23
Figure 14: Steam temperature at the upper tube exit during discharging for the nominal diameter DN 20.	24
Figure 15: Heat transfer rate of the LH-TES unit during discharging for the nominal tube diameter DN 10 .	24
Figure 16: Heat transfer rate of the LH-TES unit during charging for the nominal tube diameter DN 20 .....	25
Figure 17: Calculated temperature and liquid fraction during discharging for different fin designs .....	26
Figure 18: Excerpt from the summary of thermodynamic states at nominal point operation.....	27
Figure 19: Excerpt from the latest draft of the flow diagram showing the SH-TESS.....	33

## List of Tables

Table 1: Thermophysical material properties of the PCM, the fins and the tubes .....	18
Table 2: Tube dimensions analyzed in the parameter study .....	18
Table 3: Parameter variations, initial values and boundary conditions analyzed in the parameter study .....	19
Table 4: Parameters, initial values and boundary conditions of the different fin designs .....	26
Table 5: Calculated volume for a single tank.....	28
Table 6: Operation parameters of LH-TES at nominal operation.....	30
Table 7: Detailed geometrical design parameters of LH-TES .....	31

## Glossary, abbreviations and acronyms

<b>HT</b>	High temperature
<b>LH</b>	Latent heat
<b>SH</b>	Sensible heat
<b>TES</b>	Thermal energy storage
<b>TESS</b>	Thermal energy storage system
<b>PCM</b>	Phase change material
<b>HTF</b>	Heat transfer fluid
<b>HTC</b>	Heat transfer coefficient
<b>HP</b>	Heat pump
<b>ORC</b>	Organic Rankine Cycle
<b>PTES</b>	Pumped thermal energy storage system
<b>RES</b>	Renewable energy source

# 1. Introduction

## 1.1. Executive Summary

The detailed design of the HT-TESS was determined in various steps. First, the nominal point operation of the laboratory prototype has been considered among the partners. Subsequently, a parameter study was performed to assess the impact of several design parameters on the performance of the LH-TES unit. Therefore, the charging and discharging circuits were simulated with a variation of the design parameters, previously identified as relevant for the study. Furthermore, the finned heat exchanger tubes, which are an integral part of LH-TES, were modified in five consecutive steps to meet the requirements of the laboratory prototype. Each step consists of a structural adaptation of the fin design and a thermodynamic analysis of the radial heat conduction and melting characteristic during charging and discharging. Based on the results of the parameter study and the thermodynamic analysis, the detailed design for the tendering of the LH-TES unit was defined. The detailed design of the SH-TESS is based on the nominal point operation. For the laboratory prototype, a two-tank solution with pressurized water as the HTF was chosen. The required tank volume was determined by a MATLAB tool which is created for the calculation of constant thermodynamic states. With this tool, the effective tank volume for a charging time of 4 hours, which allows for conducting a full charging and discharging cycle within one working day, was calculated. Then, the tendering documents for the HT-TESS components were created and subsequently published on the Tenders Electronic Daily (TED) portal of the European Union.

## 1.2. Purpose and Scope

The objective of Task 3.2.1 and Task 3.2.2 is the design and build of the high temperature thermal energy storage system for the CHESTER laboratory loop. This deliverable includes the design process and the tendering of the storage system.

## 1.3. Methodology

For this deliverable, the design goals were first determined. Thereafter, a design concept was developed and the various design parameters analyzed. This allowed for the final design of the storage system and tendering of the components.

## 1.4. Structure of the document

This document is divided in three main sections.

Section 2 describes the overall thermal energy storage system and its components, as well as the main design parameters defined for the thermodynamic analysis and the specification of the high temperature storage system (HT-TESS). In addition, the basic design concept of the latent heat thermal energy storage (LH-TES) and sensible heat thermal storage (SH-TES) is described.

Section 3 presents the complete thermodynamic analysis and modelling of the HT-TESS. This includes a description of the numerical models used for a parameter study of the LH-TES component as well as the thermodynamic analysis of the finned heat exchanger tubes and the sensible heat thermal energy storage system (SH-TESS).

Finally, section 4 presents the summary of the detailed design of the HT-TESS components and a description of the tendering process, which is part of manufacturing.

## 1.5. Relations with other deliverables

This work package and deliverable is closely related to both the work package WP3.1 (D3.2) and WP3.3 (D3.4), as well as WP5 (D3.7), as the components being developed in the first two and WP3.2 are being tested together in WP5.

## 2. Description of the Thermal Energy Storage System

### 2.1. General description of the HT-TESS

The CHESTER system concept, as described first in Steinmann [1] and Jockenhöfer et al. [2], is a specific pumped thermal energy storage system (PTES) variant based on Rankine cycles using either water or organic media as the working fluid combined with a latent heat storage unit. In such systems, when excess electricity is available from a grid (usually from RES), a thermal cycle is used to transform low temperature heat into high temperature heat, which is stored in a high temperature thermal storage during charging. During periods of high electricity demand, the thermal energy stored is used to operate a power cycle to produce electricity. By thermal energy integration, the system can also act as an energy hub, providing thermal energy for the district heating sector.

Within the CHESTER project, a system that consists of three main components is considered: a high-temperature heat pump (HT-HP), a high-temperature thermal energy storage system (HT-TESS) and an Organic Rankine Cycle system (ORC). Figure 1 shows a basic scheme of such CHESTER system.

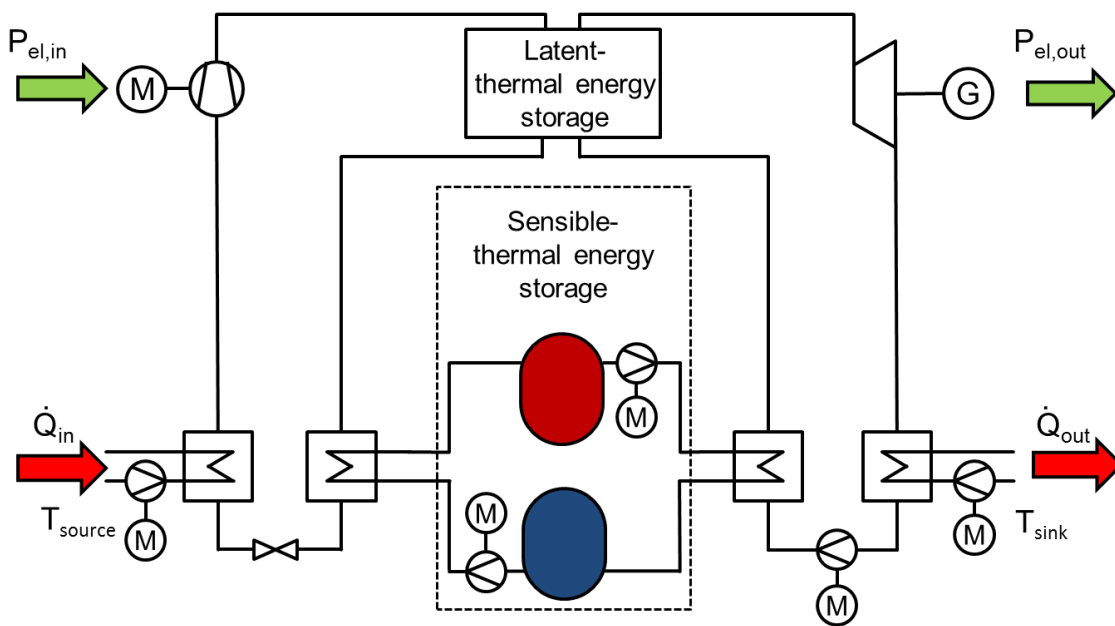


Figure 1: Conceptual diagram of the HT-TESS

The HT-TESS considered in the Chester project consists on a cascade of a LH-TESS and a SH-TESS. The LH-TESS is used as condenser for the HT-HP during charging and as an evaporator for the ORC during discharging. The subcooling or rather the preheating is provided by the SH-TESS.

## 2.2. Definition of the main design parameters

The first step in the design process of the HT-TESS is the definition of the thermodynamic boundary conditions at the inlet and outlet ports of the System. Therefore, the partners agreed on a nominal operation point for the laboratory prototype and delivered the relevant thermodynamic data. The boundary conditions for the charging cycle of the HT-TESS are defined by the thermal output and working fluids thermodynamic conditions at the optimal operation point of the heat pump. The discharging characteristics of the HT-TESS were matched to the requirements of the power cycle. The charging and discharging time was chosen to allow for a full charging and discharging cycle within one working day. As the HT-HP and the ORC use different working fluids and to avoid migration of the compressor and expander lubricant, it became necessary to develop a LH-TESS with two separate working fluid loops.

The summary of the thermodynamic boundary conditions is depicted in Figure 2.

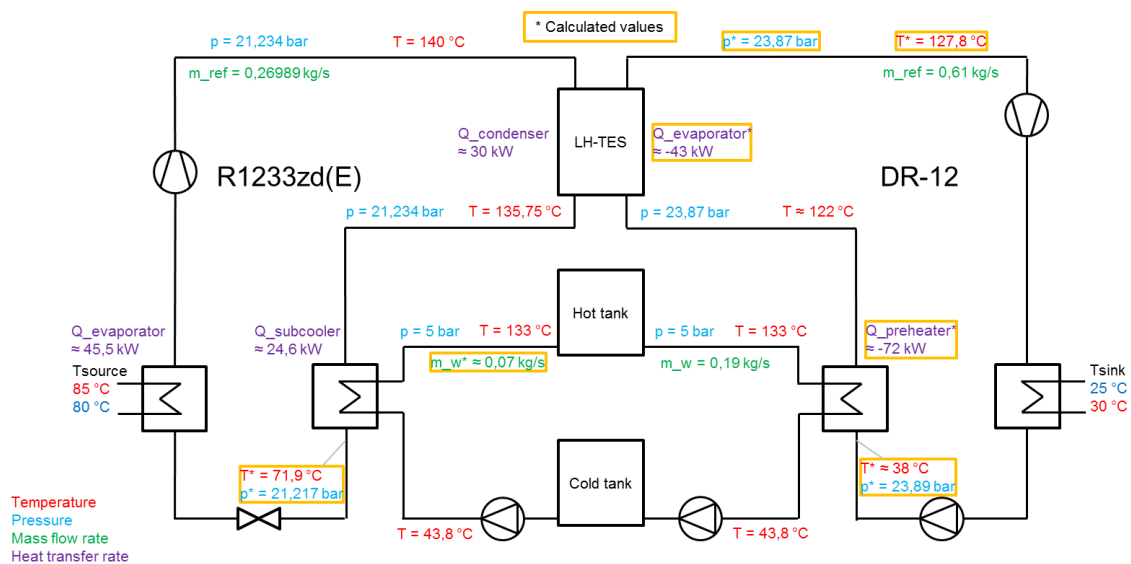


Figure 2: Summary of thermodynamic states at nominal point operation

## 2.3. Basic design concept definition

### 2.3.1. Latent heat thermal energy storage (LH-TESS)

The LH-TESS uses the phase change enthalpy between the liquid and solid phase to store thermal energy at a constant temperature. As also the working fluids are undergoing a phase change in the storage during charging and discharging at the hot side of the cycles, a LH-TESS allows for a minimal temperature difference for the heat transfer and therefore minimal entropy production. Suitable phase change materials (PCMs) in the required temperature range are nitrate salts, in this case an eutectic mixture of lithium and potassium nitrate (67 w%  $\text{KNO}_3$  – 33 w%  $\text{LiNO}_3$ ) with a melting temperature of 133 °C was chosen. Eutectic mixtures show no tendency for subcooling and do not have a melting range. Furthermore, the considered mixture has a high specific phase change enthalpy of 167 kJ/kg.

The thermal energy is transferred to and from the storage material via a tube bundle heat exchanger. The challenge in designing the heat exchanger is the low thermal conductivity of the nitrate salts. Figure 3 depicts the fundamental heat transfer mechanism in a LH-TESS during

discharging by means of a longitudinally cut through a tube with the working fluid on the inside and the phase change material PCM on the outside.

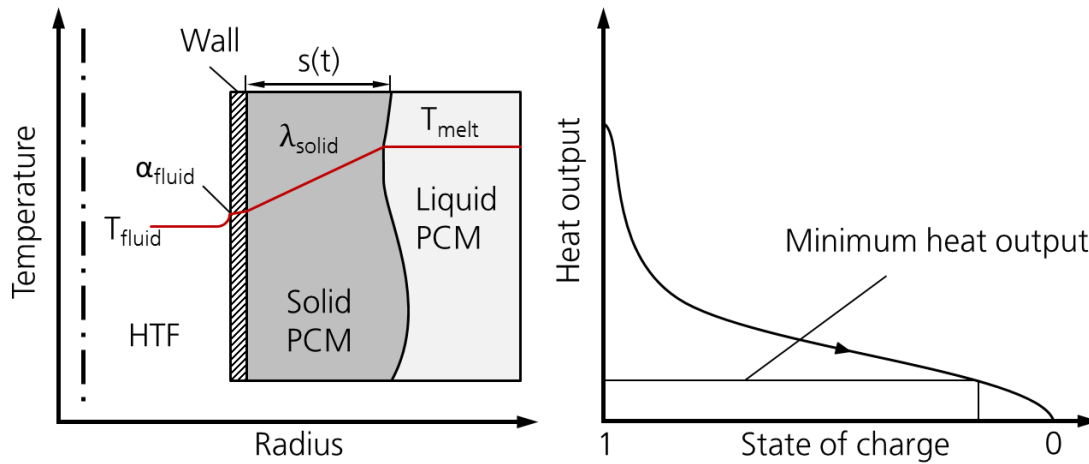


Figure 3: Fundamental heat transfer mechanism in a LH-TES during discharging and typical operation characteristics

During the solidification, the phase change enthalpy is released at the boundary area between the liquid and the solid PCM at the phase change temperature  $T_{melt}$  and has to be transferred through the already solidified layer of PCM with the heat conductivity  $\lambda_{solid}$  to the working fluid. At the beginning of the discharging cycle this layer is very thin so the limitation of the heat transfer by the thermal conductivity of the PCM only has a minor effect on the heat transfer rate. But with progressing discharge the thickness of the layer increases and thus also the heat transfer resistance caused by the PCM's heat conductivity. As a result, the thermal output of the storage at a constant temperature difference between the melting temperature and the evaporation temperature of the working fluid decreases. If the heat output decreases below the required minimum the storage is considered to be discharged. However, residual thermal energy remains unused in the storage. To achieve a constant heat output, the temperature difference between working fluid and melting temperature could be increased. This however would lead to sliding pressure operation and increased entropy production. For this reason, heat transfer structures made from extruded axial aluminum fins or pressed radial fins are used to increase the effective heat conductivity. Figure 4 shows a tube with radial fins on the left and two designs with axial fins in the center and on the right. The finned tube in the center is designed for a charging and discharging time in the hour range, the design at the right is optimized for discharging durations in the minute range at very high thermal output.

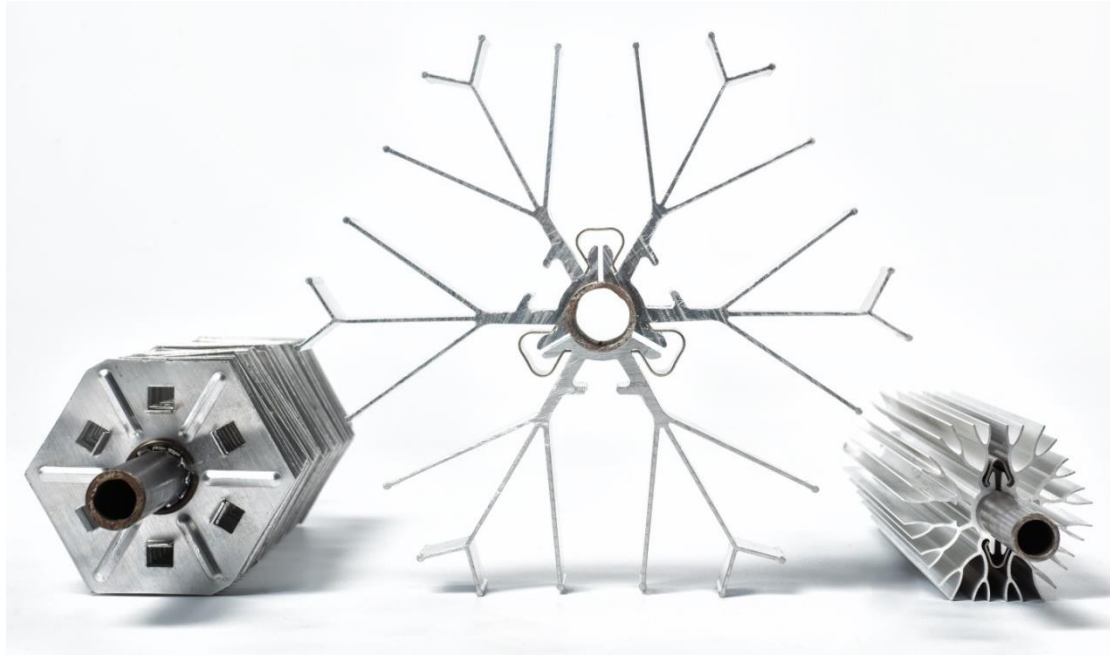


Figure 4: Radial (left) and axial (center and right) finned tubes for LH-TES application (source DLR)

The charging and discharging characteristic of a LH-TES is furthermore decisively influenced by the operation strategy of the storage. In general, two borderline cases can be distinguished, which are sketched by means of a discharging cycle.

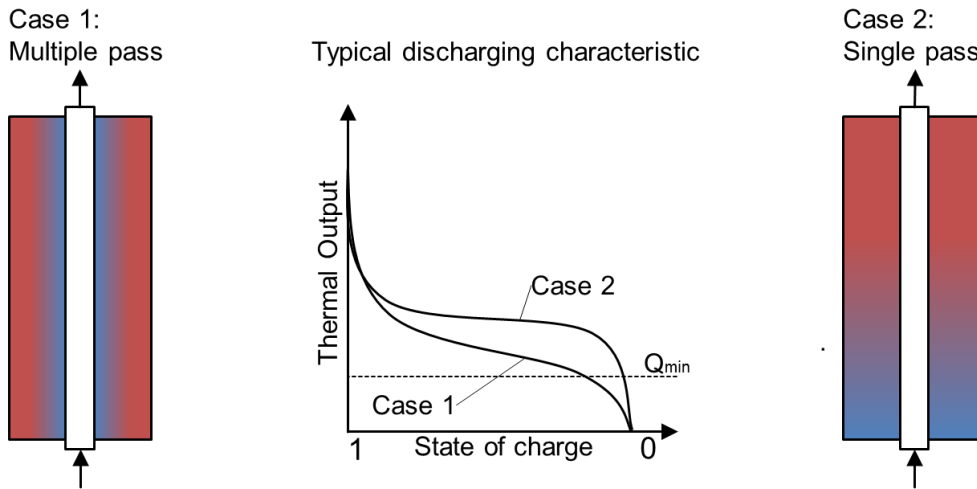


Figure 5: Impact of operation strategy (multiple pass and single pass) on LH-TES characteristic

In the first case, the tube bundle is operated similar to a natural convection steam generator with multiple passes of the working fluid. The working fluid is fed to the heat exchanger from the bottom-end and evaporates partially. The working fluid exits the heat exchanger at the top end in a two-phase state. In a steam drum the gas phase is separated from the liquid phase, which is fed back to the heat exchanger. The heat exchanger is filled over the entire length with saturated fluid at approximately constant temperature. Hence, the temperature difference between the fluid and the melting temperature is constant, too. The solidification front therefore moves radially outward. Without further measures the heat transfer rate is strongly dependent on the state of charge. Also with this concept it is not possible to provide

superheating from the LH-TES. However, the advantage of this concept is the utilization factor of the heat transferring surfaces.

In the second case the storage is discharged in single pass operation. The fluid enters the heat exchanger at the lower end and is fully evaporated at the outlet. Subsequently, the fluid is superheated until the gas temperature is equal to the temperature of the liquid PCM. Without a driving temperature gradient, the heat transfer stagnates. As a result an axial solidification front forms, which moves from the bottom to the top of the LH-TES. The thermal output and the thermodynamic state of the gas at the exit of the storage remains constant until the front reaches the upper end of the heat exchanger. In contrast to the first case, only a fraction of the heat exchanger surface is effectively used for the heat transfer. In this operation strategy the heat exchanger needs to have more surface than actually required for the desired thermal output. In a real storage there will be a combination of these two borderline cases.

Figure 6 shows a simplified sketch of a storage unit for water steam supply, developed in another project. The outer shell contains the PCM, while the heat exchanger is an integral part of the storage. The working fluid is distributed by header pipes, designed to evenly supply the tubes with working fluid. The entire unit is wrapped with thermal insulation to keep losses to a minimum.

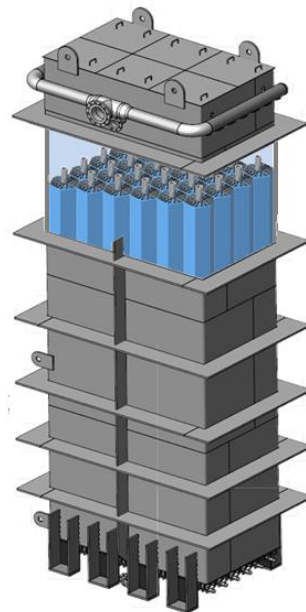


*Figure 6: Simplified schematic of a latent heat thermal energy storage based on a storage unit developed in another project (Contract number 03ESP011, ©FW Brökelmann)*

From the basic design concept analysis, the following specifications could be identified, which have to be considered for the thermodynamic analysis and the detailed design of the LH-TES unit.

- Storage configuration with vertical heat exchanger tubes and axial aluminum fins optimized for short charging and discharging durations similar to Figure 6.
- Separated heat exchanger circuits for the HT-HP and the ORC.
- Single pass operation strategy.

### 2.3.2. Sensible heat thermal energy storage (SH-TES)

The sensible heat of the working fluids from subcooling and for preheating is stored in a pressurized two-tank water storage system. During the charging process, water from the cold tank is pumped to the subcooler of the heat pump and subsequently stored in the hot tank at high temperatures. During discharging, the water from the hot tank is fed to the ORC preheater. For a detailed description of the SH-TES, see paragraph 4.2.

From the basic design concept analysis the following specifications could be identified, which have to be considered for the thermodynamic analysis and the detailed design of the SH-TESS.

- Storage configuration with two pressurized water tanks.
- Nitrogen pressure control system allowing isobaric water level variations to avoid evaporation and migration of the water during charging and discharging.
- Heating and cooling system for each tank, required to adjust the initial temperature during the test procedures in WP5.

### 3. HT-TESS Thermodynamic Analysis and Modelling

Due to the transient effects in the phase change material (PCM) during charging and discharging, the numeric modelling of the HT-TESS was mainly focused on the LH-TES unit. For the detailed design of this component, a thermodynamic analysis of the internal heat exchanger and a parameter study to determine the required storage configuration was carried out. The Layout of the SH-TESS is based on the nominal point operation which was defined for the CHESTER prototype by the WP3 partners. Since the operation parameters in this component are almost constant during charging and discharging no transient simulation was required.

#### 3.1. LH-TES

##### 3.1.1. Development and extension of numerical models

A MATLAB-based numerical model for the transient simulation of thermal energy storage with phase change materials developed by DLR was adapted and extended to the requirements of the CHESTER prototype within Task 3.2. Due to the branched geometry of the internal heat exchanger and the evaporation and condensation processes of the working fluid, the temporal and spatial variation of the heat transfer in the LH-TES unit is very complex. Thus, the model is divided in two parts. For the storage material and the heat exchanger a simplified effective model is derived from a detailed **storage model** and discretized on a finite volume mesh. The working fluid in the heat exchanger is modeled with quasi-steady one-dimensional **flow model**. In order to simulate the overall storage unit both models are coupled.

##### Storage model

The temperature  $T$  in whole LH-TES unit during charging and discharging is determined by solving the transient conservation of energy for each control volume.

$$\frac{\partial T}{\partial t} = \nabla(\alpha(\nabla T)) \quad (1)$$

The conservation of energy is described by the energy equation (1) with temperature-dependent material properties. The thermal diffusivity  $\alpha = \lambda/(\rho c_p)$  is the thermal conductivity  $\lambda$  divided by the density  $\rho$  and the specific heat capacity  $c_p$  at constant pressure.

In order to consider the phase change in the storage material the model is based on a modified variant of the enthalpy method, which is described in [3]. Thus, the governing equation (2) is directly formulated for the temperature  $T$  with the source term for the phase change.

$$\frac{\partial T}{\partial t} = \nabla(\alpha(\nabla T)) - \frac{L}{c_p} \frac{\partial f(T)}{\partial t} \quad (2)$$

This modification allows the modeling with spatially variable material properties. The latent enthalpy released or absorbed during the phase change is the product of the latent heat of fusion  $L$  and the liquid phase fraction  $f$  which is related to the melting temperature  $T_m$ .

$$f = \begin{cases} 0, & T < T_m \text{ (solid)} \\ 0.1, & T = T_m \\ 1, & T > T_m \text{ (liquid)} \end{cases}$$

Due to the rotational symmetry of the storage components, the three-dimensional system can be described in two dimensions by using cylindrical coordinates, with the radial coordinate  $r$ , the height  $z$  and the azimuthal coordinate  $\phi$  which is assumed as a constant value of  $2\pi$ . Based on this, the governing equation is discretized on a structured finite volume mesh. An exemplary illustration of the spatial discretization with a control volume and its adjacent neighbors is shown in Figure 7.

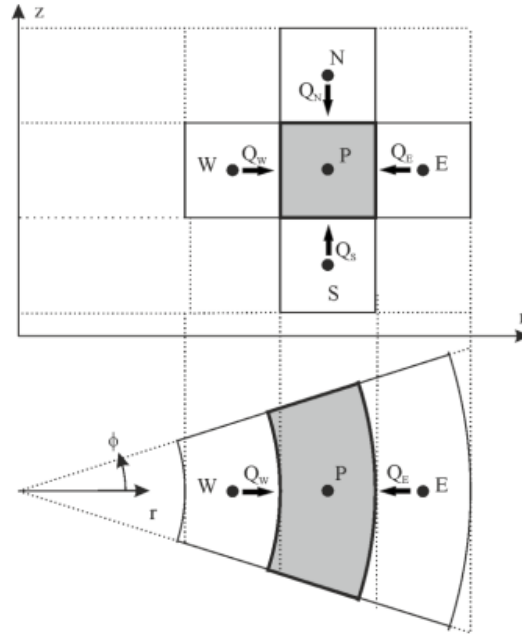


Figure 7: Side view and top view of a control volume in cylindrical coordinates [4]

The spatial discretization is derived from the energy balance of the node in the control volume with the index P, while the adjacent neighbors are denoted by the indices N, W, S and O. Volumes containing both PCM and heat transfer structures are considered with effective material properties. The effective density, specific heat and latent heat are then calculated with respect to the fraction of the heat transfer structures.

### Flow model

Model equations of a quasi-steady two-phase flow model were compiled by Keller [5]. The one-dimensional model for the working fluid in the heat exchanger tubes is described by three conservation equations. The continuity equation (3) formulated for a constant mass flux  $G$  along the tube length.

$$\frac{\partial G}{\partial z} = 0 \quad (3)$$

The momentum equation (4) reduced to a pressure drop relation including terms for acceleration ( $A$ ), gravity ( $G$ ) and friction ( $F$ ).

$$\frac{\partial p}{\partial z} = \left(\frac{\partial p}{\partial z}\right)_A + \left(\frac{\partial p}{\partial z}\right)_G + \left(\frac{\partial p}{\partial z}\right)_F \quad (4)$$

And the energy equation (5) with a convective term for the conservation of energy (left) and a volumetric heat flow rate source term (right).

$$G \frac{\partial h}{\partial z} = \frac{q'' A}{V} \quad (5)$$

$A$  is the cylindrical surface area of the heat exchanger tube. The heat flux  $q'' = q''_{FC} + q''_B + q''_C$  is calculated by a single phase forced convection term, a two-phase boiling term and two-phase condensation term.

The governing equations are discretized on a one-dimensional finite difference mesh as illustrated in Figure 8.

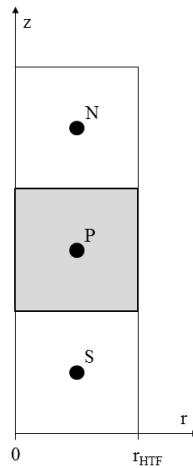


Figure 8: Spatial discretization of the two-phase flow model on the control volume nodes  $N$ ,  $P$  and  $S$

For each model, an implicit temporal discretization of the first order finally leads to a linear system of equations. The solutions from both models are coupled after each iteration. The solution is considered as converged if residual of the system of equations exceeds a defined maximum value. The adjustment of the time step size is automatically controlled by the number of required iterations and dimensionless key figures.

### 3.1.2. Parameter study of latent heat storage component

In order to assess the impact of specific design options on the performance of the LH-TES unit a parameter study was carried out. In the first step, the following parameters were identified, based on the specifications of the basic design analysis in paragraph 2.3.1, to have a significant impact on the storage performance.

- Number of heat exchanger tubes.
- Tube length.
- Tube diameter.
- Heat transfer coefficient (HTC) from the working fluid to the PCM.

Both the storage characteristic and the capacity are directly related to the number of tubes and the tube length. However, since the tube length is limited by the dimensions of the laboratory, this parameter is assumed as a constant value of 3 m, which is considered to be sufficient for the validation of the numerical model. For a given mass flux, the tube diameter affects the flow properties which have an impact on the heat transfer from the working fluid to the PCM. On the other hand the choice of a larger tube diameter could also be an additional option to increase the inner surface area through which the heat is transferred. The heat flux through this surface area depends on the HTC and the temperature difference between the working fluid and the

PCM. Currently, there is no validated correlation for the discharging processes and the chosen working fluid available which could be implemented to the **storage model**. For the charging process a correlation for film condensation was implemented to the **flow model**, which is described by Chen et al. [6]. Since this correlation also is not validated for the chosen working fluid, the results should be considered as comparative values. Thus, the impact of different HTC's was analyzed in this study. However, the temperature difference is a result of the temperatures calculated during the simulation after each time step.

The second step was the simulation of the charging and discharging process with a variation of the previously described parameters. The simulations were performed by using the MATLAB model, which was introduced in paragraph 3.1.1. The thermophysical material properties of the PCM, fins and tubes are shown in Table 1.

*Table 1: Thermophysical material properties of the PCM, the fins and the tubes*

Material property	Unit	PCM KNO <sub>3</sub> – LiNO <sub>3</sub> eu	Fin Al 6060	Tube 16Mo3
$\rho$	kg/m <sup>3</sup>	1900	2700	7850
$c$	J/(kg K)	1500	1020	482
$k$	W/(m K)	0,5	210	42,5
$T_{solid}$	°C	132,99	-	-
$T_{liquid}$	°C	133,01	-	-
$L$	J/kg	167270	-	-

For the simulations, the PCM was assumed to have constant values for density  $\rho$ , specific heat capacity  $c$  and thermal conductivity  $k$  whether if it's in the liquid state or in the solid state. However, for the thermomechanical engineering the volumetric changes have to be considered. Suitable tube dimensions for the heat exchanger design are shown in Table 2.

*Table 2: Tube dimensions analyzed in the parameter study*

Parameter	Unit	Value	Value	Value
Nominal diameter	-	DN 10	DN 15	DN 20
External diameter	mm	17,2	21,3	26,9
Internal diameter	mm	12,6	16,1	21,7
Wall thickness	mm	2,3	2,6	2,6

Based on nominal point operation, an overview of the parameter variations with the appropriate initial values and boundary conditions is given in the following tables. For charging R1233zd (E) and for discharging DR-12 is considered as the working fluid. In addition, the parameters at the inlet of the LH-TES are assumed to be constant during the simulations.

Table 3: Parameter variations, initial values and boundary conditions analyzed in the parameter study

Parameter	Unit	Value						
Number of tube pairs	pcs	70	75	80	85	90		
Tube length	m			3				
Nominal diameter	-	DN 10		DN 15		DN 20		
Mass flow rate, charging				0,27				
Mas flow rate, discharging	kg/s			0,61				
Inlet pressure, charging				21,23				
Inlet pressure, discharging	bar			23,87				
Inlet temperature, charging	°C			140				
Inlet temperature, discharging	°C			122				
Initial storage temperature, charging	°C			122				
Initial storage temperature, discharging	°C			140				
Heat transfer coefficient condensation	W/(m <sup>2</sup> K)	500	1000	Chen	2000	4000	8000	
Heat transfer coefficient boiling	W/(m <sup>2</sup> K)	500	1000	-	2000	4000	8000	

**Results for the charging process**

During charging, the working fluid enters the LH-TES unit at the upper inlet in the superheated state and condenses as it flows downwards through the heat exchanger tubes. The results of the parameter study are explained for the nominal tube diameter DN 10. Subsequently, the differences are exemplified by a comparison with the results for the nominal tube diameter DN 20. Figure 9 shows the calculated temperatures of the working fluid at the lower tube exit during charging for the nominal tube diameter DN 10. As shown in the legend of the diagram, results with the same number of tubes are marked by identical line styles and each color indicates a specific HTC.

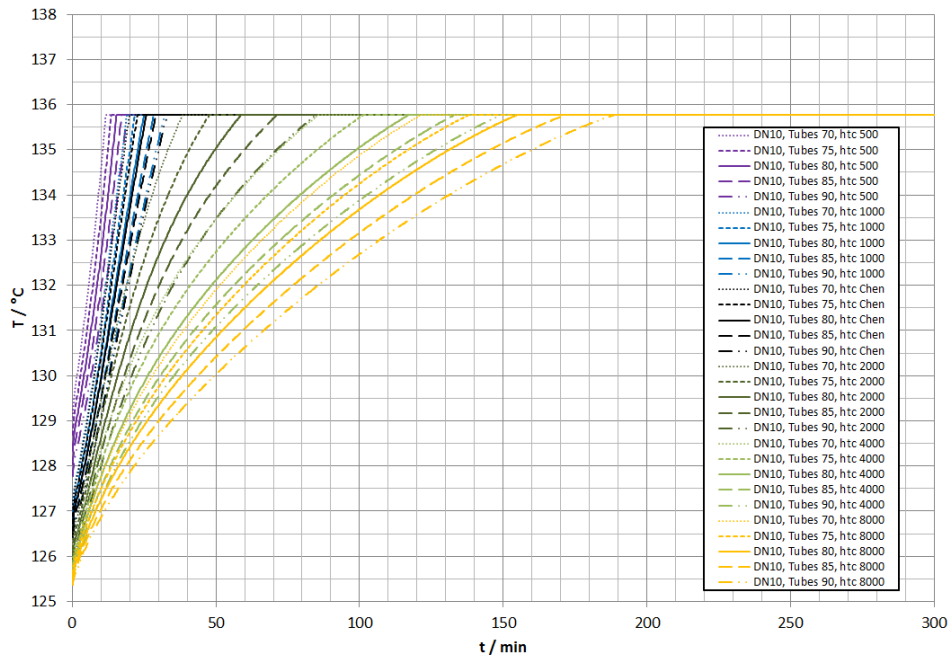


Figure 9: Temperature of the working fluid at the lower tube exit during charging for the nominal diameter DN 10

Initially, the working fluid at the exit of the tube is in the liquid state and has a temperature in the range of 125 °C to 129 °C, depending on the respective parameter variation. Then the temperature increases with the time. After a charging time of approximately 12 minutes, the variant with 70 tubes and a condensation HTC of 500 W/(m<sup>2</sup> K) reaches the evaporation point. This means, from this point two-phase flow occurs at the lower tube exit. The variant with 90 tubes and a condensation HTC of 8000 W/(m<sup>2</sup> K), on the other hand, reaches the evaporation after a charging time of approximately 188 minutes. This means by increasing the number of tubes and / or for higher condensation HTC, the onset of the two-phase flow is shifted to the right side which leads to an extension of the charging time with subcooled working fluid at the outlet of the tube. According to the correlation for film condensation (black lines) the calculated HTC for this variant is about 1000 W/(m<sup>2</sup> K).

For comparison, the results for the nominal tube diameter DN 20 are depicted in Figure 10.

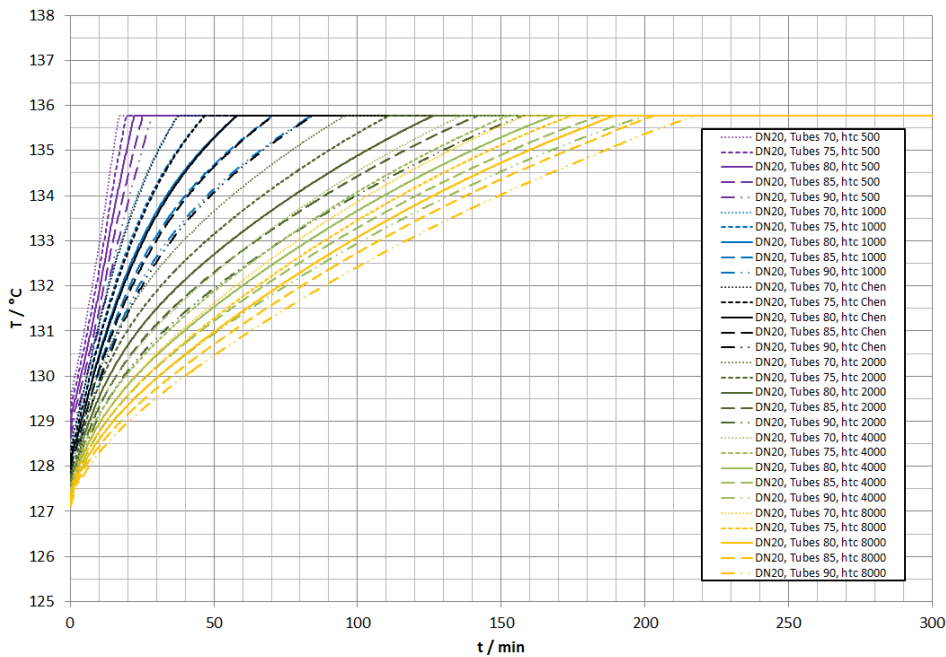


Figure 10: Temperature of the working fluid at the lower tube exit during charging for the nominal diameter DN 20

In contrast to the results shown in Figure 9, the increased tube diameter leads to a slightly higher fluid temperature at the beginning of the charging process. Also the curves are shifted to the right side which extends the charging time without two-phase flow at the lower tube exit.

Figure 11, shows the results for the heat transfer rate during charging for nominal diameter DN 10. As before, the results with the same number of tubes are marked by identical line styles and each color indicates a specific HTC.

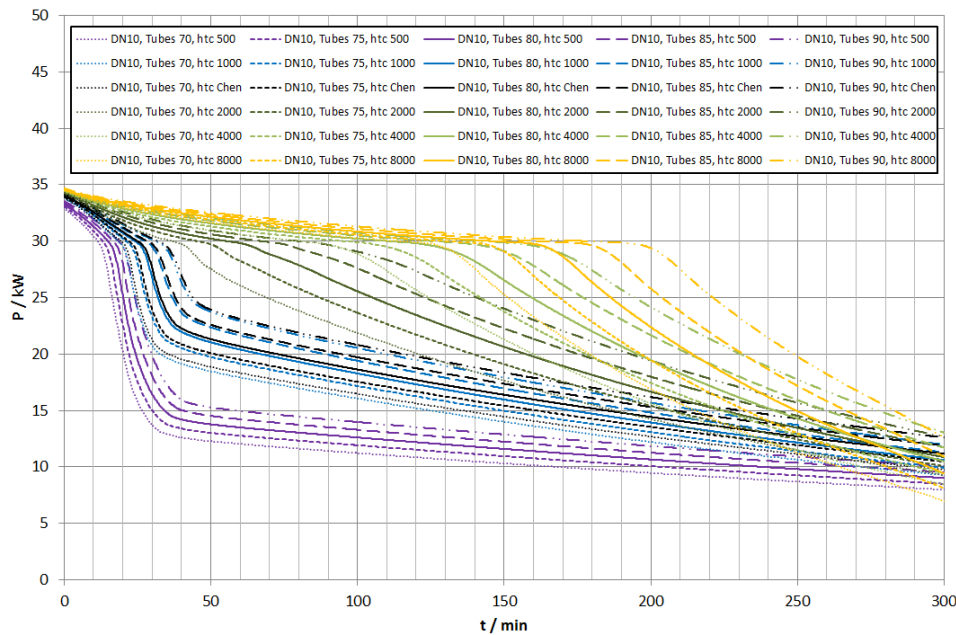


Figure 11: Heat transfer rate of the LH-TES unit during charging for the nominal tube diameter DN 10

At the beginning of the charging process, almost the entire tube length is used for the condensation of the working fluid. This results in a heat transfer rate in the range of 32 kW to 35 kW. Then the heat transfer rate decreases as the phase change area moves downwards with the time and the state of charge. As soon as two-phase flow occurs at the lower outlet of the heat exchanger, there is a significant drop in the heat transfer rate, especially for the variants with low HTC. This drop is caused by the incomplete condensation of the working fluid and by several effects in the liquid storage material.

For comparison, the results for the nominal tube diameter DN 20 are shown in Figure 12.

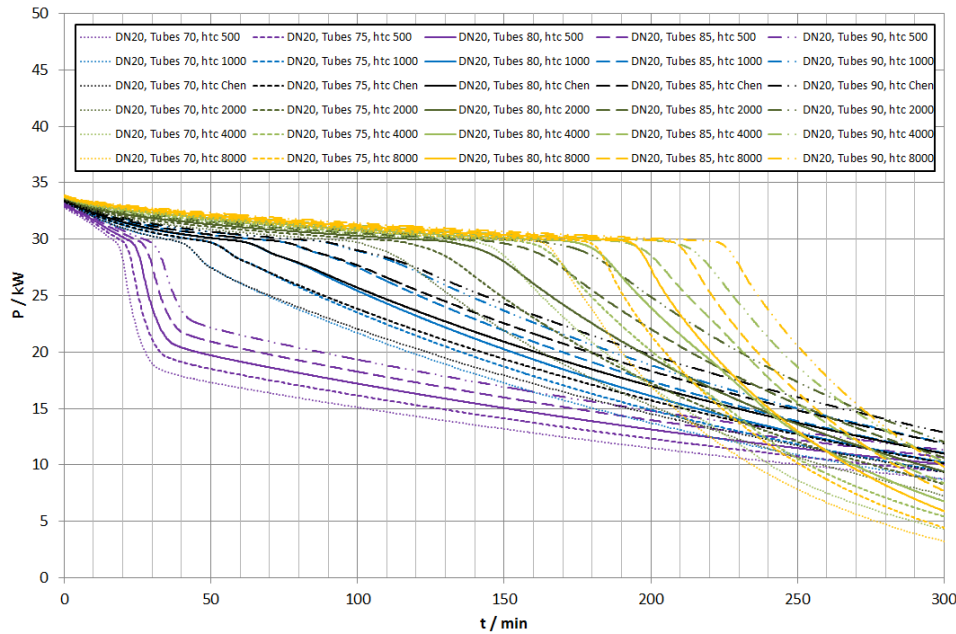


Figure 12: Heat transfer rate of the LH-TES unit during charging for the nominal tube diameter DN 20

The heat transfer rate at the beginning of the charging process is almost similar to results depict in Figure 11. Especially for the variants with a condensation HTC of 500 W/(m<sup>2</sup> K) and 1000 W/(m<sup>2</sup> K), where it can be appreciated that the drop of the heat transfer rate is less significant. Also, the curves are shifted to the right side which extends the charging time with an almost constant heat transfer rate.

### Results for the discharging process

During discharging, the working fluid enters the LH-TES unit at the lower inlet in a barely subcooled state and evaporates as it flows upwards through the heat exchanger tubes. In order to avoid two-phase flow at the inlet of the expander, the working fluid should be in the superheated state at the outlet of LH-TES unit. In this parameter study a minimum temperature of 128 °C including 5 K for superheating was considered, which is marked by the red line. As before, the results with the same number of tubes are marked by identical line styles and each color indicates a specific HTC. Figure 13 shows the calculated temperatures of the working fluid at the upper tube exit during discharging for the nominal tube diameter DN 10.

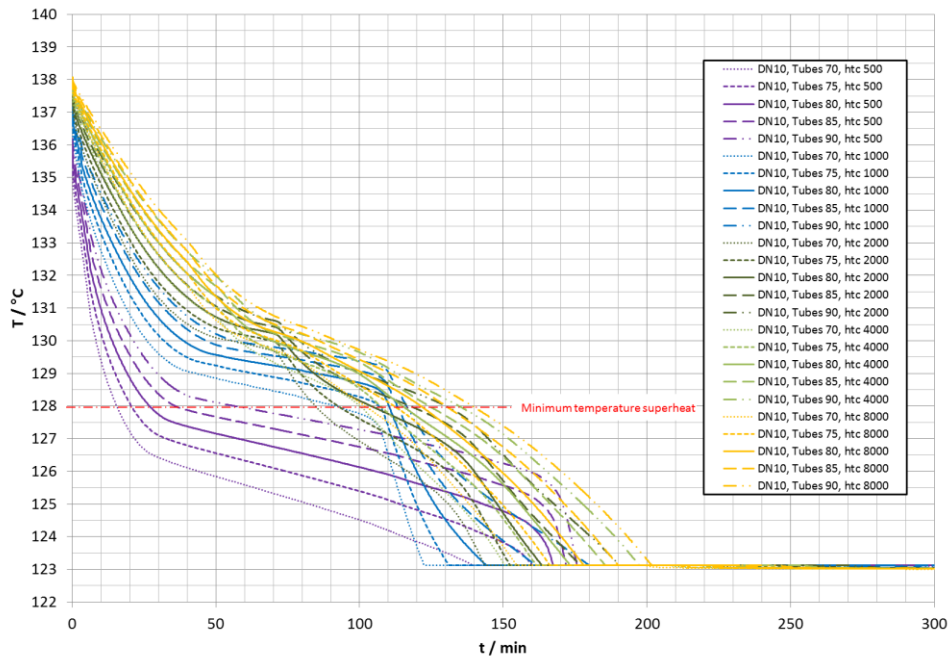


Figure 13: Steam temperature at the upper tube exit during discharging for the nominal diameter DN 10

Initially, the working fluid at the outlet of the heat exchanger tubes is in the superheated state and has a temperature in the range between 135 °C to 138 °C depending on the variant. The Variant with 70 tubes and a boiling HTC of 500 W/(m<sup>2</sup> K) falls below the minimum temperature of superheat after a discharging time of approximately 15 minutes. In contrast, the variant with 90 tubes and a boiling HTC of 8000 W/(m<sup>2</sup> K) reach this point after a charging time of approximately 138 minutes. This means by increasing the number of tubes and / or for higher boiling HTC, the curves are shifted to the right which extends the discharging time until the minimum temperature of superheat is reached.

For comparison, the results for the nominal tube diameter DN 20 are shown in Figure 14.

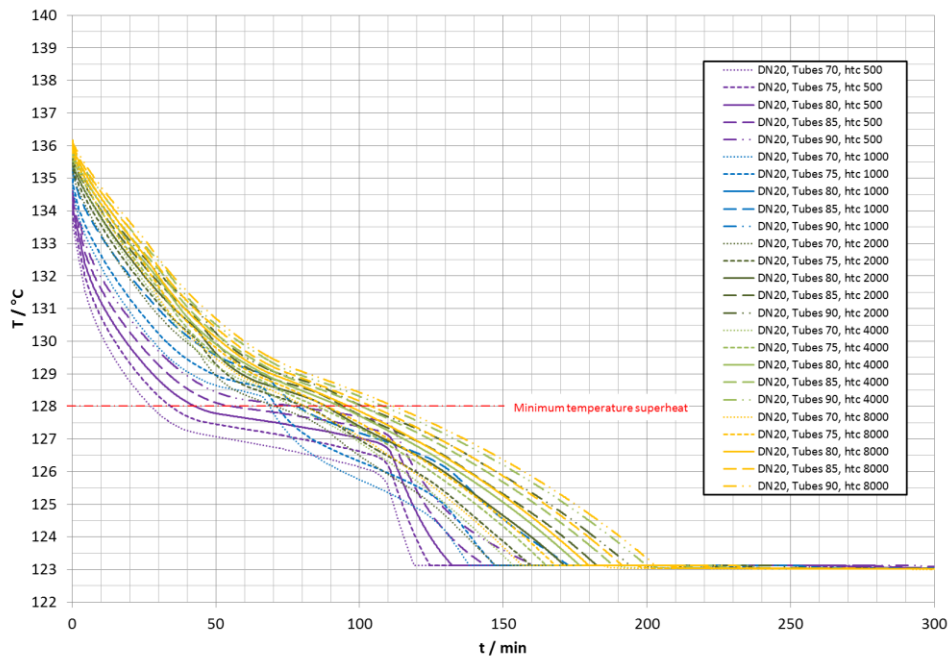


Figure 14: Steam temperature at the upper tube exit during discharging for the nominal diameter DN 20

With the nominal tube diameter DN 20, the variant with 70 tubes and a boiling HTC of 500 W/(m<sup>2</sup> K) reaches the minimum temperature of superheat after a discharging time of approximately 27 minutes, whereas the discharging time for the variant with 90 tubes and a boiling HTC of 8000 W/ (m<sup>2</sup> K) is reduced to approximately 111 minutes.

Figure 15, shows the results for the heat transfer rate during discharging for nominal diameter DN 10. As before, the results with the same number of tubes are marked by identical line styles and each color indicates a specific HTC.

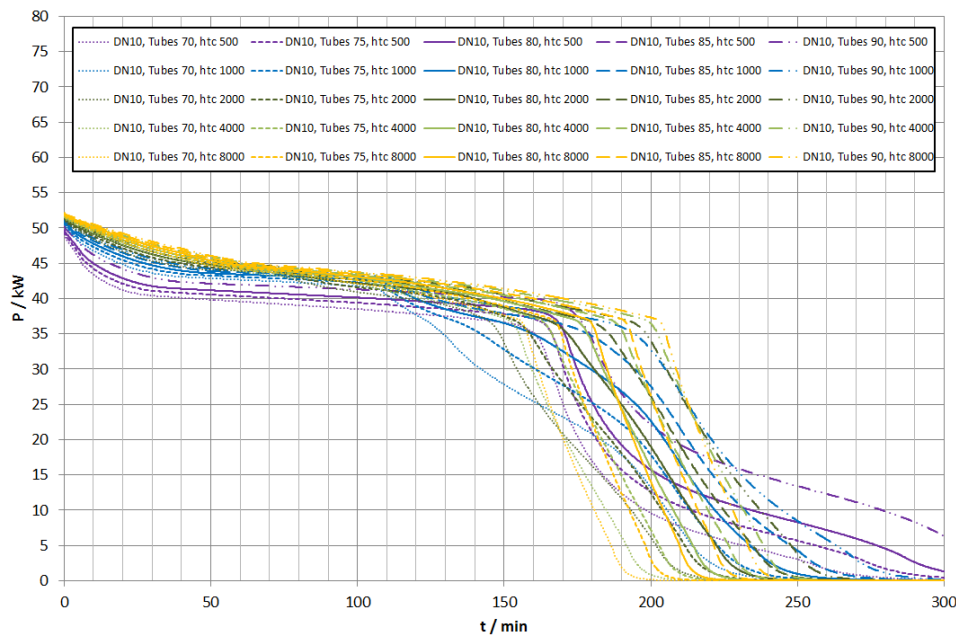


Figure 15: Heat transfer rate of the LH-TES unit during discharging for the nominal tube diameter DN 10

During discharging, a heat transfer rate of 49 kW to 52 kW is reached initially. Then the heat transfer rate decreases slowly with the time, due to the growing layer of solidified PCM on the outer surface area of the heat exchanger tubes. If the area with the two-phase flow reaches the upper tube exit, the heat transfer rate drops significantly. Then the entire length of the tube is filled with two-phase flow at an approximately constant temperature. Thus, the solidification front in the PCM moves only in radial direction at an almost constant temperature difference between the melting point of the PCM and two-phase flow.

For comparison, the results for the nominal tube diameter DN 20 are shown in Figure 14.

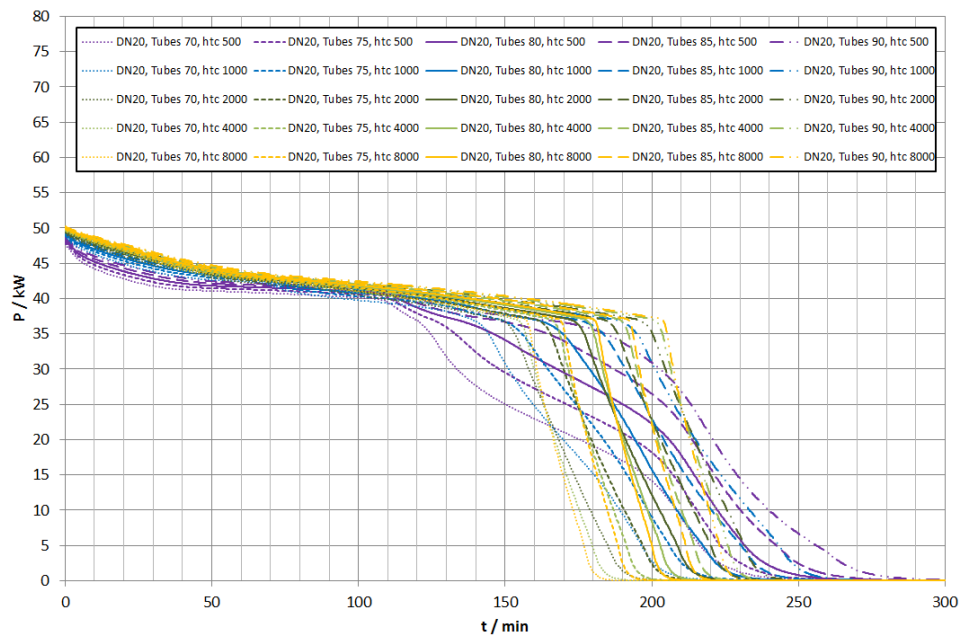


Figure 16: Heat transfer rate of the LH-TES unit during charging for the nominal tube diameter DN 20

The results for the nominal tube diameter DN 20 show only minor differences. In the variants with a low boiling HTC, the points at which the heat transfer rate drops are shifted slightly.

### 3.1.3. Thermodynamic analysis of the finned tubes

The aim of this analysis was the modification of the axial finned tube design which is shown in Figure 4 (right) to meet both the thermodynamic and the manufacturing requirements of the LH-TES laboratory prototype. The modification was carried out in five consecutive steps, which includes a structural adaption of the fin design and a thermodynamic analysis of each variant. The thermodynamic analysis was performed by using the commercially available software package ANSYS Fluent 19, which is a fluid flow solver for arbitrary unstructured meshes. For each variant, the detailed design of one finned heat exchanger tube embedded in a hexagonal PCM volume is modeled on a two-dimensional unstructured grid. Then only the energy equation transformed with the enthalpy method is solved to analyze the radial temperature distribution and the evolution of the liquid fraction during charging and discharging. In the simulations the wall temperature of the tube remains constant. Table 4 provides an overview of the parameters, initial values and boundary conditions considered for the thermodynamic analysis.

Table 4: Parameters, initial values and boundary conditions of the different fin designs

Parameter	Unit	V1	V2	V3	V5
Nominal diameter, charging	-	DN 10	DN 10	DN 10	DN 20
Nominal diameter, discharging	-	DN 10	DN 10	DN 10	DN 10
Fraction of fin	%	19,6	19,7	20,5	21,5
Initial temperature PCM, charging	°C			128	
Initial temperature PCM, discharging	°C			138	
Wall temperature tube, charging	°C			138	
Wall temperature tube, discharging	°C			128	
Melting point PCM	°C			133	

Variant V4 is not listed in Table 4, because the adapted fin design cannot be produced by the manufacturer for technical reasons.

The results of the thermodynamic analysis are shown in Figure 17 using the discharging process as an example. The curves “Temp V5 final” and “liqfrac V5 final” are representing the volume-average temperature (including tubes, fins and PCM) and the liquid fraction for the latest fin design V5. The results for previous variants are marked by the dashed lines.

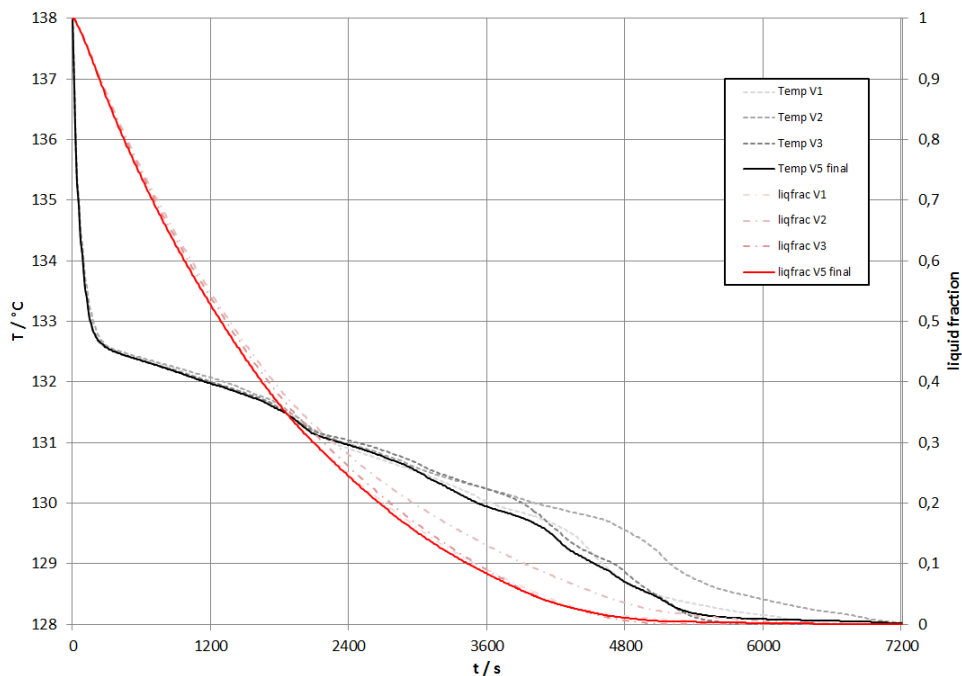


Figure 17: Calculated temperature and liquid fraction during discharging for different fin designs

Initially, the temperature decreases significantly until the melting point of the PCM is reached. After a discharging time of approximately 250 seconds the drop of the temperature is diminished due to the growing layer of solidified PCM on the surface of the finned tubes and the

resulting increase in thermal resistance. At the beginning of the discharging process, the whole PCM is in the liquid state. Subsequently, the liquid fraction in the volume-element decreases with the time. The gradient of the red curves depends on the corresponding heat flux between tube and PCM. The evolution of the curves shows a slightly increase of the heat extraction over time.

From the parameter study of the storage and the thermodynamic analysis of the finned tubes, the design variant V5 was identified to be considered for the detailed design of the LH-TES unit.

## 3.2. SH-TESS

### 3.2.1. Thermodynamic analysis of the SH-TESS

Based on the specifications of the basic design analysis in paragraph 2.3.2, the SH-TESS consists of a hot and a cold tank which are connected to the subcooler of the HT-HP and the preheater of the ORC by a closed circuit. Pressurized water was chosen as the heat transfer fluid (HTF). For the design of the storage system a MATLAB tool was created. With this tool the relevant thermodynamic state variables are calculated for charging and discharging at nominal point conditions. An excerpt from Figure 2 with the underlying thermodynamic states and the calculated values is shown in Figure 18.

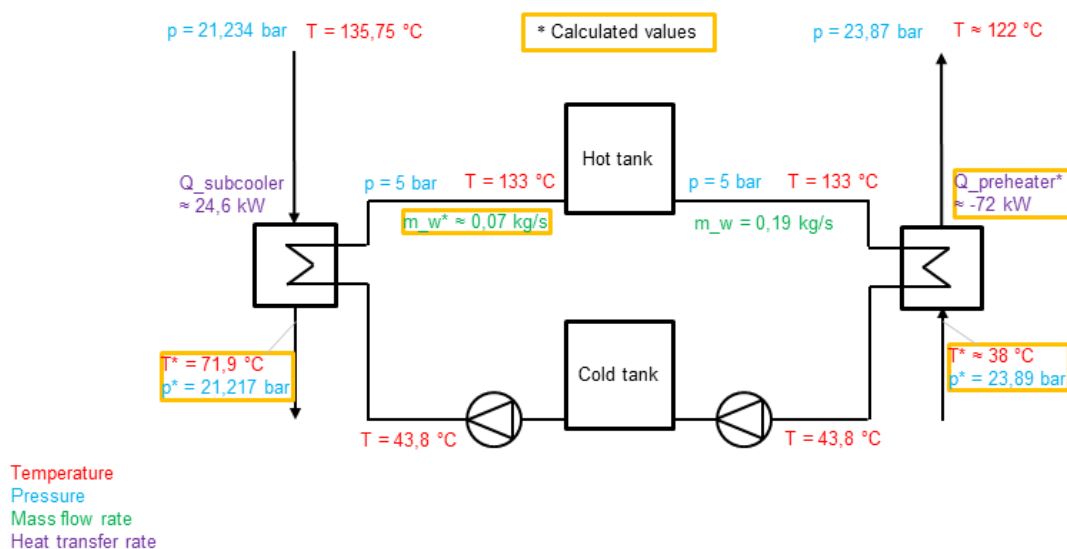


Figure 18: Excerpt from the summary of thermodynamic states at nominal point operation

The most essential design parameter is the tank volume, because this is the limiting factor during charging and discharging. For the determination of required tank volume, a constant temperature difference of 3 K between the working fluid at subcooler inlet and the HTF at subcooler outlet is assumed. This is one of the possible control strategies for the charging process which was previously defined together with the WP3 partners. The result is a constant mass flow rate of 0,07 kg/s in the water circuit. In order to perform a full charging and discharging cycle in one working day a maximum charging time of 4 hours is assumed as a boundary condition. The appropriate results for a single tank are given in Table 5.

Table 5: Calculated volume for a single tank

Parameter	Unit	Value
Effective volume (charging time 4 hours)	m <sup>3</sup>	1,012
Minimum fluid level volume	m <sup>3</sup>	0,100
Additional safety volume	m <sup>3</sup>	0,556
Minimum tank volume	m <sup>3</sup>	1,667

The effective volume is required for a charging time of 4 hours at nominal point conditions. To protect the pumps, a minimum fluid level is considered, which remains in the tank after discharging. A safety factor of 50 % is added to the previously mentioned volumes in order to take possible boundary effects into account. The sum yield in a minimum tank volume of 1,667 m<sup>3</sup> required for each tank of the SH-TESS.

### 3.3. Discussion

#### 3.3.1. Parameter study of the LH-TESS

The results of the parameter variations were analyzed separately for charging and discharging. For HT-HP loop with the working fluid R1233zd (E), the nominal tube diameter DN 20 leads to an extended charging time with subcooled working fluid at the outlet of the heat exchanger tube. This is probably related to the increase of the inner surface area of the tube through which the heat can be transferred. However, this only applies to a charging process at constant inlet conditions. At sliding pressure operation or variable mass flow rates this effect could be less distinctive. Due to the results of the correlation for film condensation, an HTC of around 1000 W/(m<sup>2</sup> K) is more likely than 8000 W/(m<sup>2</sup> K). Nevertheless, this value can only be considered as a rough estimation, as the correlation has not been validated for the chosen working fluid yet. For the ORC loop with the working fluid DR-12, an increase in the tube diameter did not lead to any appreciable change in the discharging characteristic of the LH-TESS unit. In general, the results show that the heat transfer is not limited by the heat exchanger and the PCM below a HTC value of 8000 W/(m<sup>2</sup> K). Furthermore, the tube number has primarily an impact on storage capacity. Secondary effects can have an influence on the heat transfer mechanism which has to be further investigated. Therefore, further measures to increase the HTC on the inside of the tube are particularly useful.

#### 3.3.2. Thermodynamic analysis of the finned tubes

The finned heat exchanger tubes are modified in five consecutive steps to meet both the thermodynamic and the manufacturing requirements. The fin design was adapted in collaboration with the manufacturer and then thermodynamically analyzed after each step. As a result, the heat extraction from the storage material could be slightly increased. However, since the aluminum fraction and the fin shape have not changed significantly, this effect is rather small. Based on the results of the parameter study, the final heat exchanger design considers the nominal tube diameters DN 20 for the charging loop and DN 10 for the discharging loop. In addition, the fins are adapted to the specific requirements of the laboratory prototype at nominal point operation.

### 3.3.3. Thermodynamic analysis of the SH-TESS

The determination of the tank volume is essential for the SH-TESS design. The calculations are based on the charging process at nominal point conditions, because the ORC operation is always limited by the state of charge. A minimum volume of 1,667 m<sup>3</sup> for a single tank is calculated for a charging time of 4 hours at constant conditions. Regarding the operation of the laboratory prototype in WP5, this parameter was chosen to perform a full charging and discharging cycle in one working day.

## 4. HT-TESS Design and Manufacturing

### 4.1. Detailed design of LH-TESS

Based on the specifications derived from the basic design concept definitions (see paragraph 2.3) and the results of the thermodynamic analysis, the LH-TESS is designed as a vertical tube and shell heat exchanger with two separate tube registers for charging and discharging. The shell side is filled with the PCM, while the tube side contains the working fluid. For the charging loop a larger tube diameter was chosen as for the discharging loop, due to the conclusions from the parameter study presented in paragraph 3.1.2. Each tube register is connected with header pipes, designed for an even fluid flow distribution and low pressure losses. The heat exchanger tubes are outfitted with axially extruded aluminum fins according to variant V 5 described in 3.1.3 to improve the effective heat transfer. The fin design was optimized for short charging and discharging durations within the thermodynamic analysis. A single pass operation is considered for both loops. During charging the gas enters the corresponding tube register from the top side and condenses at the tube inside as it flows downwards. The working fluid feed from the ORC enters the tube register at the lower inlet during discharging and is evaporated upward along the tube length. Besides regarding the density changes between liquid and vaporous working fluid, the change in flow direction is necessary to reduce thermomechanical stress due to the solidification of the PCM and the specific volume changes during the phase change. The PCM containing shell side is open to the atmosphere. The operation parameters of the LH-TESS are summarized in Table 6.

*Table 6: Operation parameters of LH-TESS at nominal operation*

Parameter	Charging loop	Discharging loop
Fluid	R1233zd (E)	DR-12
Absolute pressure	0-33 bar(a)	0-36 bar(a)
$T_{min}$	20 °C	20 °C
$T_{max}$	165 °C	165 °C
$m_{nom}$	0,27 kg/s(gas)	0,61 kg/s(liq.)
$V_{norm, inlet}$	7,85 m <sup>3</sup> /h(gas)	2,55 m <sup>3</sup> /h(liq.)
$m_{min}$	0,02 kg/s(gas)	0,31 kg/s(liq.)
$V_{min, inlet}$	0,58 m <sup>3</sup> /h(gas)	1,27 m <sup>3</sup> /h(liq.)
$m_{max}$	0,50 kg/s(gas)	0,61 kg/s(liq.)
$V_{max, inlet}$	14,53 m <sup>3</sup> /h(gas)	2,55 m <sup>3</sup> /h(liq.)

Table 7 shows the detailed geometrical design parameters of the tube register and the containment used for the tendering.

Table 7: Detailed geometrical design parameters of LH-TES

Heat exchanger	
Type	Tube bundle with separate circuits for charging and discharging
Heat exchanger configuration	Vertical tube pairs integrated to the PCM volume and connected to the headers
Operation strategy	Single pass
Nominal tube diameter, charging loop	DN 20
Nominal tube diameter, discharging loop	DN 10
Minimal length of finned tubes between headers	3,0 m
Tube material	16Mo3
Number of tube pairs	ca. 90 pcs.
Axial fins	
Fin design	Variant V 5 optimized for short charging and discharging durations
Fin material	Aluminum 6060
Fraction of fin volume	22 %
Expected header configuration	
Upper header, charging loop	Horizontal
Lower header, discharging loop	Horizontal, with a height of 0,5 m between the floor of the laboratory and the tube connection
Storage	
Maximal height of LH-TES unit	5,2 m
Shell material	16Mo3
PCM Volume, liquid state	≈ 1,4 m <sup>3</sup>

The exact number of tube pairs depends on the design of the headers as well as the final arrangement of the tube register and will be determined during the tendering process.

For the required tube and shell material 16Mo3 a corrosion allowance of 1 mm on surfaces with contact to the PCM is sufficient.

## 4.2. Detailed design of SH-TESS

Figure 19 shows an excerpt of the prototypes flow diagram depicting the SH-TESS. During the charging cycle water from the cold tank B201 is pumped to the subcooler W103. The heated water is stored in the hot tank B202. Excess heat can be extracted from the heat pump to the lab cooling system via a bypass. The SH-TESS can be decoupled in this case. This operation mode can be necessary during initial start-up and conditioning of the HT-TESS. During discharging hot water from tank B202 is provided to the preheater of the ORC. The cold water is fed back to the tank B201. In both cycles, the mass flow of the water is controlled by the outlet temperature of the heat exchangers. As the hot tank temperature exceeds the saturation temperature at ambient pressure, each tank is designed as pressure vessels with a minimum volume of 1,667 m<sup>3</sup>. To compensate for volume changes due to the varying water levels, both tanks are equipped with a nitrogen pressure control system, to keep the tank pressure above the saturation pressure. Due to the different temperatures and the corresponding difference in the partial pressure of the water, it is not suitable to just connect the tanks with a compensating pipe. This would lead to migration of water from the hot to the cold tank. For the initial start-up and reconditioning between experiments, both tanks can be tempered with immersion heaters and an internal heat exchanger connected to the lab cooling network. To obtain a complete charge of the LH-TES with a spatially equal temperature as start-up boundary condition, while the SH-TES is already fully charged, it is necessary to continue to operate the heat pump. In this case, the subcooler can be disconnected from the SH-TES tanks. Instead the excess thermal energy is rejected to the lab cooling system via the bypass lines 001 and 002. The overall control strategy including the three main components heat pump, TES and ORC will be developed at a later time during the project. As the tanks are designed as pressure vessels, safety valves for each tank are required. All heaters are going to be fitted with safety temperature limiters according to the DGRL and AD 2000 requirements.

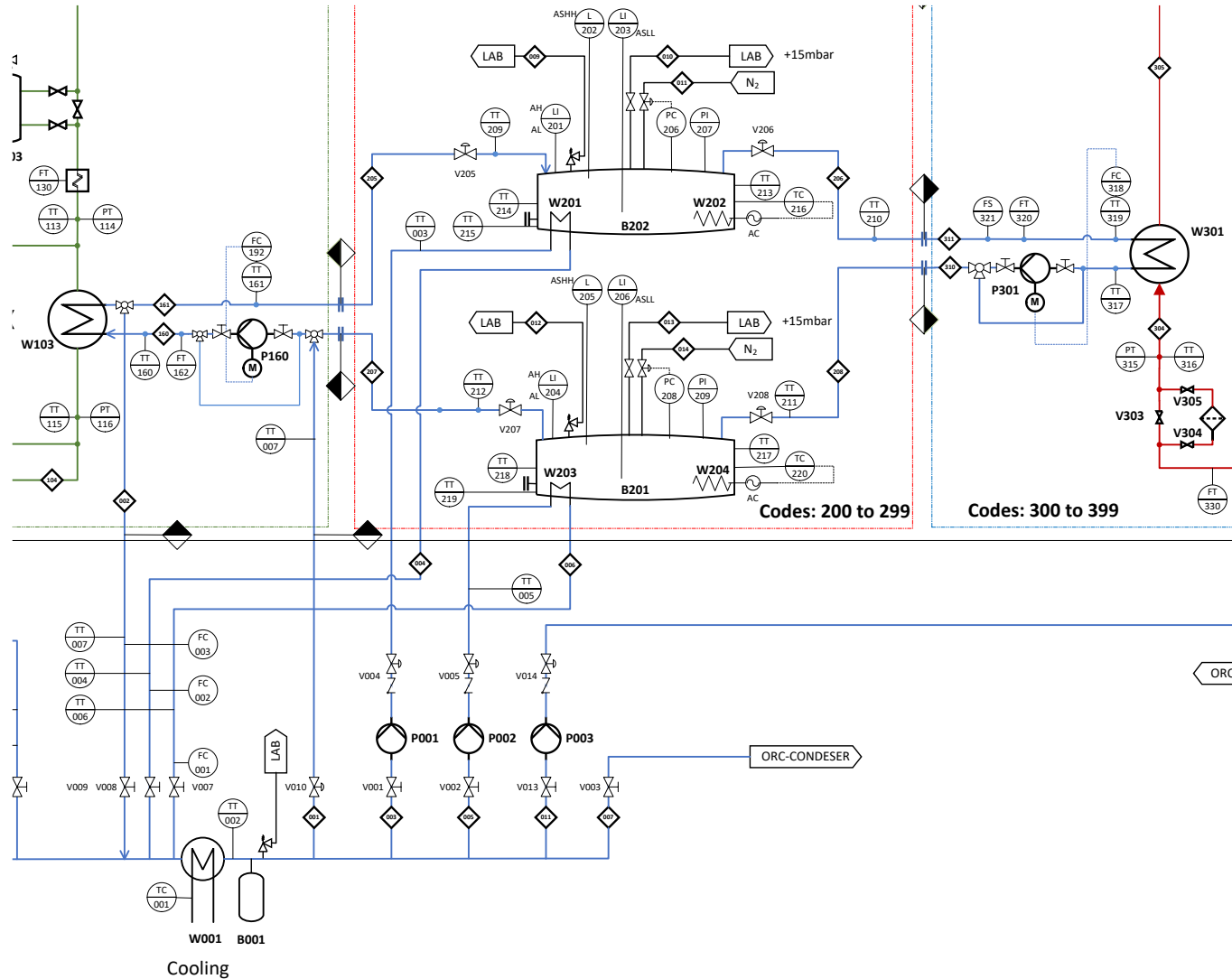


Figure 19: Excerpt from the latest draft of the flow diagram showing the SH-TESS

### 4.3. Manufacturing of the HT-TESS

The tendering of the HT-TESS is carried out separately for the LH-TES and the SH-TES. Initially, tendering documents must be prepared with an appropriate specification of each component. Subsequently, the tendering documents will be published on the Tenders Electronic Daily (TED) portal of the European Union. The EU procurement procedures involve the following stages.

#### **Pre-qualification**

In the first stage, bidders must submit a request for participation and have to prove their qualifications. Deadline for the submission of applications for the pre-qualification are 30 days. This is followed by an internal assessment of the pre-qualified candidates which takes about 7 days.

#### **Bid period**

In the second stage, the pre-qualified candidates prepare their offers, which must be submitted within 25 days. This is followed by open meetings to negotiating the final contract terms. Subsequently, bidders can submit an optimized offer. The deadline for submitting the optimized bids can be defined by DLR.

#### **Bid evaluation and internal processing**

The third stage includes the analysis and evaluation of the offers followed by an internal processing period of approximately 2 to 3 weeks.

#### **Contract Execution**

In the fourth stage the contract is signed with the winner of the tendering process.

At the time this report was created, the tendering process of the HT-TESS was ongoing.

## 5. Conclusions

A parameter study was performed to assess the impact of several design parameters on the performance of the LH-TES unit. Therefore, the charging and discharging circuits were simulated with a variation of the design parameters, previously identified as relevant for the study. It turned out that an increase of the tube diameter leads to an extended charging time with subcooled working fluid at the outlet of the heat exchanger tube. However, this effect was not apparent during discharging. The results showed that the heat transfer is not limited by the heat exchanger and the PCM below a HTC value of  $8000 \text{ W}/(\text{m}^2 \text{ K})$ . Also, the tube number has a primarily impact on storage capacity. Nevertheless, the influence of secondary effects on the heat transfer mechanism has to be further investigated. In order to meet requirements of the laboratory prototype the finned heat exchanger tubes are modified in five consecutive steps. Each step consists of a structural adaption of the fin design and a thermodynamic analysis of the radial heat conduction and melting characteristic during charging and discharging. Based on the results of the parameter study and the thermodynamic analysis, the detailed design for the tendering of the LH-TES unit was defined.

The detailed design of the SH-TESS is based on the nominal point operation of the laboratory prototype defined by the WP3 partners. For the laboratory prototype a two-tank solution with pressurized water as the HTF was chosen. The storage system consists of a hot and a cold tank which are connected to the subcooler of the HT-HP and the preheater of the ORC. The required tank volume was determined by a MATLAB tool which is created for the calculation of constant thermodynamic states. With this tool the effective tank volume for a charging time of 4 hours was calculated. In addition a safety factor and minimum fluid level, which remains in the tank after charging or discharging, were taken into account. Furthermore, a hydraulic bypass in the water circuit is considered to extract excess heat from the HT-HP. This operation mode can be necessary during initial start-up and conditioning of the HT-TESS.

The detailed design of the HT-TESS components was specified for the tendering documents. Subsequently, the tendering documents were created and published on the Tenders Electronic Daily (TED) portal of the European Union.

## References

- [1] W. D. Steinmann, „The CHEST (Compressed Heat Energy STorage) concept for facility scale thermo mechanical energy storage,“ *Energy*, Bd. 69, pp. 543-552, <https://doi.org/10.1016/j.energy.2014.03.049>, 2014.
- [2] H. Jockenhöfer, W. D. Steinmann and D. Bauer, „Detailed numerical investigation of a pumped thermal energy storage,“ *Energy*, Bd. 145, pp. 665-676, <https://doi.org/10.1016/j.energy.2017.12.087>, 2018.
- [3] V. R. Voller, „Fast Implicit Finite-Difference Method for the Analysis of Phase Change Problems,“ *Numerical Heat Transfer, Part B: Fundamentals*, Bd. 17:2, pp. pp. 155-169, DOI: 10.1080/10407799008961737, 1990.
- [4] J. Vogel, „Simulation eines zylindrischen latenten thermischen Energiespeichers in MATLAB,“ internal report DLR, 2013.
- [5] M. Keller, „Modellierung der Zweiphasenströmung in senkrechten Röhren für die Anwendung von PCM-Speichern in solarthermischen Kraftwerken mit Direktverdampfung,“ Karlsruher Institut für Technologie (KIT), DOI: 10.5445/IR/1000087340, 2014.
- [6] S. L. Chen, F. M. Gerner and C. L. Tien, „General Film Condensation Correlations,“ *Experimental Heat Transfer: A Journal of Thermal Energy Generation, Transport, Storage, and Conversion*, pp. 93-107, DOI: 101080/08916158708946334, 1987.